CONF-880724--22

DE88 012065

# CHARACTERIZATION OF FLOW REGIMES IN THE POST-DRYOUT REGION

N. T. Obot
Dept. of Chemical Engineering
Clarkson University
Potsdam, New York 13676
(315) 268-7735/6650

M. Ishii
Reactor Analysis & Safety Division
Argonne National Laboratory
9700 South Cass Avenue
Argonne, Illinois 60439
(312) 972-4586

## ABSTRACT

A visual study of film boiling using photographic and high speed motion-picture methods was carried out to determine the flow regime transition criteria in the post-CHF region. An idealized inverted annular flow was obtained by introducing a liquid jet of Freon 113 through a nozzle, precisely centered with respect to the internal diameter of the test section, with an annular gas flow. The respective ranges for liquid and gas exit velocities were 0.05-0.5 and 0.03-8.2 m/s. Nitrogen and helium were used in the study.

## NOMENCLATURE

| | |
|---|---|
| $A_i$ | Constant, defined by Eq. (3) |
| $B_i$ | Constant, defined by Eq. (4) |
| $C_i$ | Constant, defined by Eq. (6) |
| Ca | Capillary number, $\mu_f V_f/\sigma_f$ |
| $D_j$ | Liquid jet hole diameter, m |
| $L_B$ | Axial extent of a flow section, m |
| V | Velocity, m/s |
| $V_{rel}$ | Relative velocity, $V_g - V_f$, m/s |
| We | Weber number, $\rho V^2 D_j/\sigma$ |
| $We_{g,rel}$ | Gas Weber number, $\rho_g V_{rel}^2 D_j/\sigma_f$ |

### Greek Symbols

| | |
|---|---|
| $\alpha$ | Void fraction at inlet to test section |
| $\mu$ | Viscosity, Pa.s |
| $\rho$ | Density, $kg/m^3$ |
| $\sigma$ | Surface tension, N/m |

### Subscripts

| | |
|---|---|
| f | Liquid |
| g | Gas |
| j | Liquid jet |
| rel | Relative, or based on $V_{rel}$ |

## I. INTRODUCTION

An inverted annular flow, which consists of a liquid core surrounded by a vapor annulus, is of considerable importance in the areas of Light Water Reactor (LWR) accident analysis, cryogenic heat transfer, and other confined, low quality film boiling applications. Although extensive studies of the heat transfer characteristics for this flow situation have been carried out by numerous researchers,[1-3] there have been very few systematic investigations of the hydrodynamics of inverted annular flow.

The main objective of the inverted annular flow research program was to determine the effects of inlet liquid and gas conditions on the flow regimes in the post CHF region. A flow visualization of a simplified film boiling configuration, consisting of a Freon 113 liquid core surrounded by a gas annulus, was made. From an analysis of the still photographs and high speed motion pictures, it was determined that there are basically four flow regimes and it was also possible to determine the axial extents of these flow zones with remarkable consistency. Predictive equations, in generalized and simplified forms, were then developed for the axial limits of the different flow regimes.

## II. REVIEW OF EXPERIMENTAL STUDIES OF POST-CHF REGION

Visual and high-speed motion picture observations of film boiling in channels have been reported by a number of researchers. For example, Chi and co-workers[4-6] considered film boiling of saturated hydrogen under transient cooling conditions and obtained the following flow regimes along the horizontal test section: annular, slug and dispersed flows. For the range of flow conditions covered in their study, Kalinin et al.[7] observed both the annular and slug flow regimes.

For upward flow of liquid nitrogen in a vertical tube, Laverty and Rohseno[illegible]

two distinct flow regimes: an annular flow with liquid in the center and vapor in the annulus occurred at the beginning of the heated section, followed by a dispersed region of filaments/droplets of liquids at greater tube lengths. In a subsequent study, Forslund and Rohsenow[9] confirmed the large departure from thermal equilibrium in the dispersed flow film boiling.

A detailed experimental study of adiabatic inverted annular flow was carried out by DeJarlais,[10] DeJarlais et al.,[11] and Ishii and DeJarlais[12] using coaxial downward flow water jets and various gases in a glass tube. The disintegration of the liquid core into droplets was found to be due to two different mechanisms: wave instabilities at the interface and roll-wave entrainment.

Since the absence of film boiling conditions (no wall wetting, droplet vaporization in the vicinity of heated wall, etc.) may limit the applicability of the adiabatic results, an extensive and consistent flow visualization study of a diabatic inverted annular flow was performed by DeJarlais, and Ishii and DeJarlais.[13-15] A simplified upward flow geometry, consisting of a liquid jet of Freon 113 surrounded by a gas annulus, was studied. In addition to the existence of an annular and dispersed flow regime, in line with the results of Laverty and Rohsenow,[8] the presence of two well-defined regimes - the agitated and the inverted slug/churn flow, was also documented. The axial extent of each flow regime, as well as the transition from one regime to another, was found to depend markedly on the relative velocity between the gas and the liquid, in agreement with the observation of Laverty and Rohsenow. No correlations were developed for the extents of the flow regimes.

The channel flow film boiling studies reviewed so far dealt almost exclusively with visual, still and movie-camera observations of the complete structure of the two-phase flow field. Although it has long been known that the prevailing film boiling regime has profound effects on heat transfer and on the hydraulic resistance, only several studies of film boiling hydraulic resistance have been reported (Kalinin et al.,[7] and Graham et al.[16]).

## III. EXPERIMENTAL FACILITY AND TEST PROCEDURES

### A. Test Apparatus

The steady state film boiling experimental facility, shown schematically in Fig. 1, consisted of a transparent quartz tube, a simplified inverted annular flow geometry formed by a round liquid jet core surrounded by an annular gas flow. The liquid jet of Freon-113 was discharged into the test section using thin-walled interchangeable stainless steel tubes (9.02 and 10.8 mm, ID), each of which was

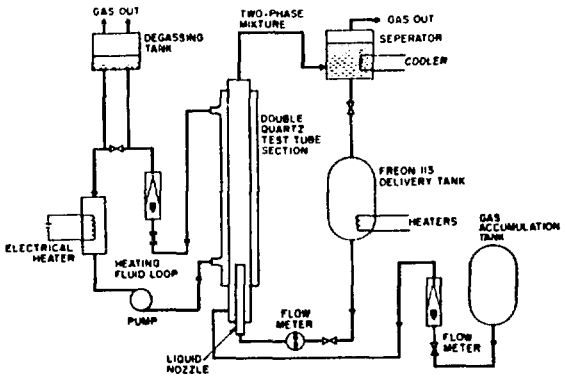


Fig. 1. Schematic of the Experimental Facility

precisely centered with respect to the internal diameter of the heated quartz tube, while the gas (nitrogen or helium) was introduced via the annular gap between the stainless steel nozzle and the quartz tube. The corresponding void fractions were 0.56 and 0.37 for $D_i$ = 9.02 and 10.8 mm, respectively. Liquid and gas flow rates were measured with turbine flowmeter and rotameters, respectively; temperatures at all critical locations being sensed with chromel-alumel thermocouples.

The heated portion of the test sections, 1.0 m in length (Fig. 2), consisted of two quartz tubes, finished in much the same way as Liebig or West condensers. The dimensions of the inner and outer quartz tubes were 16 x 13.6 mm OD/ID and 35 x 31 mm OD/ID, respectively, giving an annular gap of 31 x 16 mm OD/ID through which a high temperature heat transfer fluid (Syltherm 80 by Dow Corning) was circulated. The inner quartz tube extended beyond the outer one to give an unheated entrance length of 150 mm (Fig. 2).

Inverted annular flow could be established in the test section by heating the heat transfer fluid above minimum film boiling temperature and then introducing saturated or subcooled test

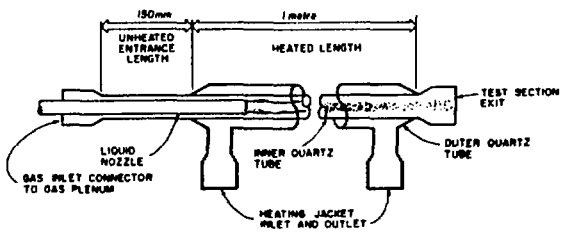


Fig. 2. Details of the Test Section

liquids such as Freon-113 into the inner tube directly. The drawback with this approach is one of lack of control of the annular gas conditions. The alternative simplified inverted annular flow geometry, one that was used for the present study and afforded accurate control of the flow conditions at the inlet to the test section, was obtained by introducing a circular liquid jet through the stainless steel tube with a surrounding annular gas flow (Figs. 1 and 2), the latter being discharged through an annular plenum located below the quartz test section.

### B. Test Procedures, Photographic Technique and Data Analysis

Preliminary preparations prior to a trial run included degassing of the freon supply tank and the establishment of the desired freon temperature by heating and/or cooling, charging of the gas accumulation tank to 60-80 psig, heating of the Syltherm loop to a stable temperature of 225-270°C, cooling of the separator tank (used to recover the freon from a two phase mixture leaving the test section) to about 0°C or lower, and a check on the lighting conditions to be used for photographic and/or motion picture observations. In these experiments, the gas was at room temperature, between 22°C and 27°C, depending on the trial run. The freon temperature, prior to delivery to the test section, was also within the above range.

During a trial run, visualization of the hydrodynamic behavior within the test section was accomplished using both still photograph and high speed motion pictures. For the former, a 35 mm SLR camera was used along with 400 ASA black and white film. Lighting was provided by either of two 3 μs strobe lights, each delivering a 0.5 w-s pulse of light. With this short exposure time, small (0.1 mm) droplets traveling at speeds above 10 m/s were observed without significant blurring of the image. The light from the strobe was bounced off a white background onto the test section.

For a given test run, a series of still photographs were taken using a 55 mm lens which provided a complete view of a 0.3 m length of the test section on each 35 mm film frame. The pictures were taken at five or six locations, spanning the full length of the test section, including the entrance and exit sections. At each location, two to five photographs were taken, giving about 10-30 frames for each trial. To obtain more detailed structure of the flow field, additional still photographs were taken with 105 mm or 200 mm lenses. Either back or side strobe lighting was used.

For some selected trials, motion pictures were taken using several different cameras and Kodak VNX 430 (400 ASA) color reversal film, with a film speed of 500 fps for most trials. Lighting was provided by four 450W flood lights, these being directed onto the same background as noted above for the still photographs. The interested reader may wish to refer to the detailed discussion of the qualification methods for optical and/or photographic techniques which is given in Ref. 13.

The last comment here deals with the data used to generate the correlations shown subsequently. These were obtained by analyzing the still photographs, taken with the 35 mm black and white film, in the following manner. The axial extents of the different flow regions were established by carefully studying the developed negatives using a light table fitted with binocular microscope, the reference scale being the image of the graduated scale (in cm) mounted alongside the test section. Liquid surface tension data used for computation of Weber number were obtained from Sinitsyn et al.[12] For drop size analysis, the negatives obtained with the 55 mm SLR lens were projected onto a screen, with a minimum negative-to-screen image magnification of 500. By this procedure the drop sizes were determined down to the 100-200 μm size range. Although determination of the flow regime or the sizes of the droplets were accomplished with little difficulty, a shortcoming is the rather time consuming frame by frame analysis. Motion pictures of the flow field were analyzed on a motion picture analyzer, with x-y plotting cross hairs and film projection speeds from 48 fps down to zero.

## IV. RESULTS AND DISCUSSION

### A. An Overview of the Hydrodynamics of the Flow Field

Prior to presentation and discussion of the results for the axial extent of the flow regimes, it is instructive to review the flow patterns that were established for this simplified inverted annular flow. This brief summary is intended to provide the reader with a clear picture of the most important characteristics of the various flow regimes, and will not contain exhaustive details.

Smooth (Small Surface Wave) Section. This smooth region begins from the nozzle exit (test section entrance) and can extend to about thirty nozzle diameters depending, of course, on the relative velocity between the gas and the liquid core. For a given liquid jet entrance velocity, the maximum length occurs at very low gas exit velocities, decreasing markedly with increasing gas velocity to almost zero at high gas velocities. The shearing effect on the liquid jet by the gas; notably, the complete elimination of a smooth section as observed in the present study at high gas velocities, parallels that usually encountered in twin fluid atomization processes.

Rough Wavy Section. With increasing distance downstream, the liquid interface becomes

wavy with nearly symmetric waves, the wavelengths of which are roughly 10 mm (order of magnitude). Except for the existence of a rough wavy interface, this region of the flow field is quite solid, with a fairly intact liquid core filling the center of the test section. As with the smooth section, its axial extent varies according to whether the gas velocity is greater or less than the liquid jet velocity. For example, with $V_{rel}$ (i.e., $V_g - V_f$) > 0, the physical length of this flow regime decreases (from about 10-20 nozzle diameters) with increasing $V_{rel}$ to the point that, at a $V_{rel}$ of about 2 m/s, both the smooth and rough wavy sections are nonexistent, the prevailing regimes being an agitated zone in the immediate vicinity of the nozzle exit and large liquid slugs/ligaments over the remaiming portion of the test section. By contrast, test trials with $V_{rel}$ < 0 resulted in lengths that were within 10-50 jet hole diameters. It is pertinent to note that in DeJarlais and Ishii,[13-15] this regime is referred to as the agitated solid core while the present agitated section, to be discussed next, corresponds to the inverted slug/churn flow in Refs. 13 through 15.

Agitated Section. With increasing downstream distance and/or at sufficiently high gas velocity, the nearly axisymmetric interfacial waves become very irregular and transform to large amplitude or roll waves. Farther from the rough wavy section or at a still larger gas velocity, significant interfacial deformation occurs, resulting in the break-up of portions of the roll-waves into ligaments and droplets. This mechanism of liquid break-up or drop formation has been treated quite well by Ishii and Grolmes[16] and DeJarlais,[10] hence the details will not be given here. Other general features of this flow regime include the formation of skirt-like annular sheets of liquid due to extreme growth and distortion of the roll-waves, the presence of highly agitated liquid annulus in the vicinity of the heated wall and of large liquid slugs in the central portion of the test section. With these general characteristics, it is quite clear that, unlike the smooth or rough wavy section, this section of the flow which may extend beyond the end of the heated portion of the test section (depending on the liquid and gas flow rates) is very unstable.

Dispersed (Ligament and Drop) Section. For the ranges of liquid and gas velocities covered in the present study, this flow regime was generally confined to the downstream locations nearest to the test section exit. For test trials with high relative velocities, i.e., $(V_g - V_f)$ > 1 m/s, the dominant feature of the downstream flow field was that of dispersed ligaments/droplets with either of the gas species. For low-to-moderate $V_{rel}$ values, many of the large liquid ligaments or slugs at the exit of the test section were very distorted. If the test section were sufficiently long, it is likely that these ligaments would eventually disintegrate into smaller, stable drops.

B. Formulation of the Generalized Correlations

From a detailed study of an adiabatic inverted annular flow,[10-12] it was established conclusively that the correlated jet break-up data followed two distinct trends; one for the region over which the jet break-up length was independent of void fraction, relative velocity or gas density, with a marked sensitivity of the break-up to these variables for the second region. The break-up lengths for these two regions were closely approximated by the following equations:

$$L_B/D_j = 480\ Re_j^{-0.53}\ We_j^{0.5} \qquad (1)$$

$$L_B/D_j = 685\ Re_j^{-0.53}\ We_j^{0.5}\ [We_{g,rel}/\alpha^2]^{-0.645} \qquad (2)$$

Since the two curves intersect at $We_{g,rel}/\alpha^2$ = 1.73, this critical value of the modified Weber number provides a useful criterion for determining the validity range for each equation. Another important finding was that the break-up mechanisms for an adiabatic inverted annular flow were similar to those documented in the literature for free jets.

On the basis of the above information, it was envisaged that the average extent of each flow regime could be correlated in terms of the nondimensional variables in Eqs. (1) and (2). Accordingly, the present data were reduced and the results are presented graphically in Figs. 3-6. The first three figures show, successively, the upper bound to the range of axial extents for the smooth, rough wavy and agitated flow sections. Beyond the agitated flow regime lies the dispersed ligaments/droplets section. The extent of this zone is shown in Fig. 6 from which it may be noted that it extends beyond the heated portion of the test section for most trials. The data used to prepare these plots are presented in tabular form elsewhere.[19]

In each of Figs. 3-6, data are shown for the two gas species (helium and nitrogen) tested. To provide useful insight on the role of relative velocity, it was considered worthwhile to further identify the data points in Figs. 3-5 according to whether the average gas velocity at the annulus ($V_g$) is less or greater than the liquid jet velocity ($V_f$) at the inlet to the test section.

Another general comment, one that is of particular importance, relates to the interpretation of the data for $L_B/D_j$. Each value of $L_B$, always measured from the nozzle exit (test section entrance), is scaled with the constant

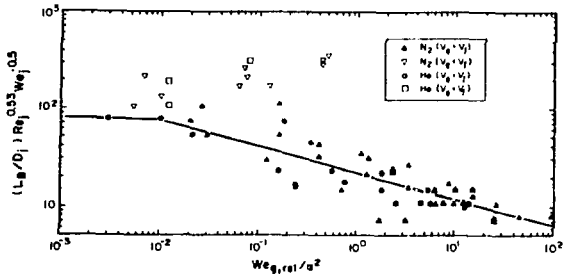

Fig. 3. Correlation for Upper Limit of Smooth Flow Section

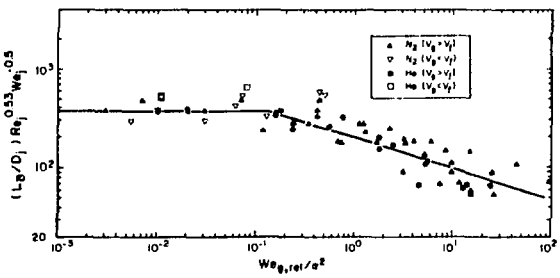

Fig. 4. Correlation for Upper Limit of Rough Wavy Section

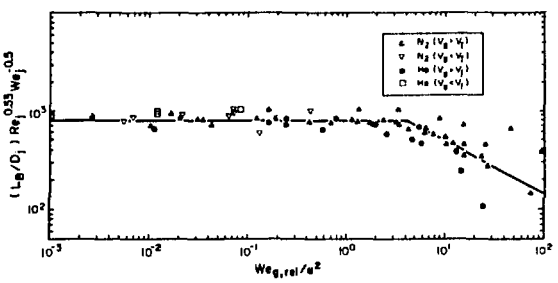

Fig. 5. Correlation for Upper Limit of Agitated Section

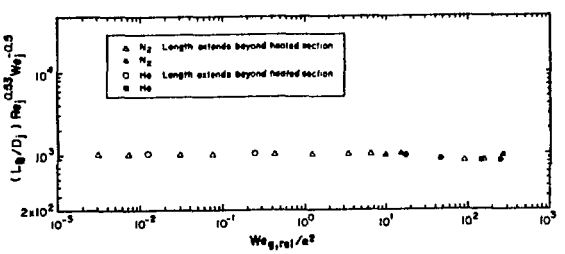

Fig. 6. Typical Extent of Dispersed Flow Section

nozzle diameter, $D_j$. Thus, depending on the liquid and gas velocity, the observed average length, $L_B/D_j$, for the rough wavy section includes that for the smooth region, while that for the agitated regime may include both the smooth and rough wavy regions. Likewise, the $L_B/D_j$ value for the dispersed zone may encompass all or some of those for the preceding upstream regimes. The data that are given in Figs. 3-6 represent average values obtained by studying the 16-20 photographic frames taken for a given set of inlet flow conditions.

The general trends on Figs. 3-6 are two-fold; a nearly constant $L_B/D_j$ value with increasing $We_{g,rel}/a^2$ for the region over which the average limits depend solely on the inlet liquid jet conditions, $Re_j$ and $We_j$, followed by steadily decreasing values with further increases in $We_{g,rel}/a^2$, which is the expected trend when $L_B/D_j$ is dependent on both liquid and gas conditions at the inlet to the test section. For the smooth section, the length of which exhibits the greatest sensitivity to variations in relative velocity, gas density and void fraction, the few data available[19] for $We_{g,rel}/a^2 < 10^{-3}$ together with those shown in Fig. 3 favor the observation that this extent is essentially independent of gas Weber number for $We_{g,rel}/a^2 < 10^{-2}$.

An exception to the trends noted above is observed to occur for the dispersed flow section (Fig. 6). Here, it will be noted that, over the *entire* $10^{-3} \leq We_{g,rel}/a^2 \leq 10^{3}$ *range*, $L_B/D_j$ *is* almost determined solely by the liquid jet Reynolds and Weber numbers, $Re_j$ and $We_j$. Conceivably, with increasing modified gas Weber number, *conditions would eventually* have been obtained for which $L_B/D_j$ would decrease markedly with $We_{g,rel}/a^2$, in line with the trends on Figs. 3-5. The general trend on this figure *appears to support this view.*

To render the results on Fig. 6 intelligible, it is necessary to discuss briefly the test conditions and the attendant flow phenomena. For the nitrogen trials, two values of liquid velocity (0.34 and 0.5 m/s) were used, while the annular gas velocity was varied between 0.52 m/s and 8.2 m/s. For $V_\ell$ = 0.5 m/s and $V_g$ = 0.52 m/s, the average limits for the smooth, rough wavy and agitated section were 2 $D_j$, 15$D_j$ and 70$D_j$, successively, while the region of dispersed flow extended beyond the heated section beginning from about 70$D_j$. Although the axial extents of the first three regions decreased markedly with almost complete depletion of the smooth zone, while the dispersed region increased, as the gas velocity was progressively increased, the latter continued to extend beyond the heated section up to $V_g \approx 4.4$ m/s. These results are so identified in Fig. 6 and, for these trials, only portions of this zone (up to the end of the heated section) were measured. For $V_g > 4.4$ m/s, the prevailing flow

in well over two-thirds of the test section was one of dispersed droplets, with flaky remnants towards the exit of the resting section, and these results are indicated with solid symbols. For the helium trials, $V_f$ was held constant at 0.34 m/s while $V_g$ was varied between 0.22 m/s and 5.6 m/s. These results have also been classified accordingly.

A closer examination of the results in Figs. 3-5 reveals one consistent trend with test trials for which the liquid jet velocities were larger than the annular gas velocities at the inlet to the test section. It may be noted that, for the smooth, rough wavy or agitated section, the axial limits for $V_f > V_g$ tend to lie above the mean regression line determined for data with $V_f < V_g$; notably for the range of $We_{g,rel}/a^2$ over which $L_B/D_j$ is only susceptible to liquid conditions. It may also be noted that the above trend is most pronounced for the smooth section, with vestiges in the rough wavy and agitated regions. The clear implication here is that viewing the results solely in terms of the absolute values of relative velocity or Weber number does not provide a very accurate picture of the axial limits of the flow regimes.

Over the range where $L_B/D_j$ is independent of $We_{g,rel}/a^2$, a linear regression using only data for $V_f < V_g$ resulted in relations of the form:

$$L_B/D_j \leq A_i \, Re_j^{-0.53} \, We_j^{0.5} \qquad (3)$$

The numerical values of the constant, $A_i$, together with the approximate ranges of validity of Eq. (3) are summarized in Table 1. From comparison of the $A_i$ values in Table 1 with the value in Eq. (1), i.e., $A_i = 480$, which was developed from adiabatic tests based on the break-up mechanism of free liquid jets, it is quite apparent that Eq. (1) would predict lengths that are somewhat higher than, but not significantly different from, the combined lengths determined here for the smooth and rough wavy sections.

When $L_B/D_j$ depends on $We_{g,rel}/a^2$, the data are approximated by:

$$L_B/D_j \leq B_i \, Re_j^{-0.53} \, We_j^{0.5} \, [We_{g,rel}/a^2]^{m_i} \qquad (4)$$

The appropriate values for $B_i$, $m_i$ along with the ranges of validity are also given in Table 1. The values for $B_i$ and $m_i$ were determined by logarithmic least squares technique and the correlation coefficients were between 0.85 and 0.9, these being as good as can be expected for carefully run experiments using a visual analysis for flow regime characterization; especially since in the case of the smooth section replicate runs sometimes resulted in lengths that differed by as much as 100%. In this regard, it is pertinent to note that the length of the smooth section rarely exceeded $2D_j$ for $V_{g,rel} \geq 0.5$ m/s. It may be noted that, for the constants $A_i$ and $B_i$ (Table 1), the last digits have been rounded to zero or five and the error introduced by this procedure is less than one percent.

## C. Simplified Correlations

The presentation in the preceding section is important in two respects. First, it provides good insight into the mechanisms that determine the axial extents of the various flow sections. And, second, good estimates of the critical gas Weber number for transition, from regions with no effect to those with marked dependence on relative velocity, can be established for nearly all of the flow sections.

For low-to-moderate gas velocities satisfying the conditions $V_g - V_f > 0$ and $L_B/D_j = f(Re_j, We_j)$, a further simplification of Eq. (3) can be made in order to provide predictive equations that may be readily applied for design calculations. Realizing that $We_j/Re_j = \mu_f V_f/\sigma_f$ (= Capillary number, $Ca_j$), Eq. (3) can be rewritten as

$$(L_B/D_j) \, Re_j^{0.5} \, We_j^{-0.5} = (L_B/D_j) \, Ca^{-0.5} < A_i/Re_j^{0.03} \qquad (5)$$

or

$$L_B/D_j \leq C_i (We_j/Re_j)^{1/2} \leq C_i \sqrt{Ca_j} \qquad (6)$$

A straightforward re-analysis of the data for each trial was carried out by dividing the already computed $A_i$ values by $Re_j^{0.03}$. For the $1{,}774 \leq Re_j \leq 13{,}279$ range covered in the present study, $Re_j^{0.03}$ varied from 1.252 to 1.330, with an average value which could be stated as $1.296 \pm 0.034$, i.e., with about a 3% variation about the mean value. Although very good estimate of the constant $C_i$ for each flow section can be obtained by simply dividing the appropriate value in Table 1 by 1.296, a linear regression using the new data set resulted in the following correlations:

Smooth section:

$$L_B/D_j \leq 60\sqrt{Ca_j}, \text{ for } (We_{g,rel}/a^2) \leq 10^{-2} \qquad (7)$$

Table I. Summary of Predictive Equations

| Flow Section | First Region+ $L_B/D_j \leq A_i\ Re_j^{-0.53}\ We_j^{0.5}$ | | Second Region+ $L_B/D_j \leq B_i\ Re_j^{-0.53}\ We_j^{0.5}\ [We_{g,rel}/\alpha^2]^{m_i}$ | | |
|---|---|---|---|---|---|
| | $A_i$ | Validity range for $We_{g,rel}/\alpha^2$ | $B_i$ | $m_i$ | Range for $We_{g,rel}/\alpha^2$ |
| Smooth | < 80 | $\leq 10^{-2}$ | 25 | -0.27 | $>10^{-2}$ |
| Rough Wavy | <380 | $\leq 10^{-1}$ | 200 | -0.31 | $>10^{-1}$ |
| Agitated | <770 | ≤3.5 | 1500 | -0.5 | >3.5 |
| Dispersed | >770 | ≤10 | - | - | |

+Range for $Re_j$ and $We_j$: $1775 \leq Re_j \leq 13{,}280$ and $4.5 \leq We_j \leq 260$.

Rough wavy section:

$$L_B/D_j \leq 295\sqrt{Ca_j},\ \text{for}\ (We_{g,rel}/\alpha^2) \leq 10^{-1} \qquad (8)$$

Agitated section:

$$L_B/D_j \leq 595\sqrt{Ca_j},\ \text{for}\ (We_{g,rel}/\alpha^2) \leq 3.5 \qquad (9)$$

Dispersed section:

$$L_B/D_j > 595\sqrt{Ca_j},\ \text{for}\ (We_{g,rel}/\alpha^2) \leq 10 \qquad (10)$$

In addition to the individual ranges specified above, Eqs. (7)-(10) are valid for $0.0028 \leq Ca_j \leq 0.02$. As with Table 1, the last digit is rounded to zero or 5. Equations (7)-(9) give estimates that are close to the values observed experimentally, with a 6-20% error band. As might be expected from the trend in Fig. 3, the largest percentage differences were calculated for the relatively short smooth section.

A final comment here deals with Eq. (10) which might appear at first to exclude the presence of a dispersed section over a third of the initial heated portion of the test section. Of the numerous trials with $V_{rel} \leq 2$ m/s, about 80% of the measured lengths satisfied Eq. (10). For all test trials with $V_{rel} > 2.0$ m/s, Eq. (10) did not apply. For instance, for two nitrogen trials with $V_{rel} = 7.6$ and 5.0 m/s, the onset of a dispersed ligament/droplet section was observed to occur at about 10-13 jet hole diameters downstream from the nozzle exit, which is considerably less than about 34 diameters that could be inferred from Eq. (10). This continual depletion of the liquid core into ligaments/droplets of liquid with increasing relative velocity, a generally expected trend, is qualitatively in agreement with the observations of Laverty and Rohsenow.[8]

D. Droplet Generation and Drop Size Distributions

Downstream of the rough wavy section, a significant portion of the liquid surface area consists of small droplets formed by roll-wave entrainment and by jet instability within the agitation region. These droplets were quite small, with sizes under 200 μm in diameter. In the immediate vicinity of the heated wall, these small droplets were probably short-lived due to very rapid vaporization.

Typical size distributions for droplets formed by roll-wave entrainment and by instability at the rough surfaces of the agitated region are shown in Fig. 7 for three trials, two (708 and 727) with helium and the other with nitrogen. To obtain these data, photographs taken with the 200 mm lens (resolution down to roughly 25 μm, but limited depth of focus) focussed at the depth corresponding to the outer (facing) surface of the liquid nozzle were analyzed. With this focussing, droplets within 2-3 mm of the heated wall nearest to the camera were in sharp focus. Droplets observed shearing from roll-wave crests or within 10 mm of the leading (downstream) edges of the agitated masses were measured, provided they were within sharp focus, the others being ignored.

For high, positive relative velocity ($V_g - V_f$), the flow field near the exit of the test section is characterized by dispersed droplets, with unstable and distorted liquid ligaments/slugs for moderate relative velocities. These droplets are largely the result of roll-wave entrainment and jet instabilities, and the

maximum drop size depends on the stability of the liquid core remnants and liquid mass in the agitated region. Typically, droplets/slugs over 3 mm were observed to be quite distorted and far from being spherical, a possible indication that these large drops (or small slugs) were unstable and would eventually disintegrate into smaller droplets in a sufficiently long test section.

Typical drop size distributions in the dispersed flow region are given in Fig. 8 for three trials, two (216 and 224) with nitrogen and the other with helium. These data were obtained by analyzing still photographs taken with the 55 mm lens (resolution down to about 100 μm). Spherical or near spherical droplets were recorded by diameter while unstable, distorted slugs were measured along long and short axes, and recorded by estimated total volume, assuming cylindrical form with the short axis corresponding to the diameter.

The following comment can be made about the results in Figs. 7 and 8. The maximum droplet size generated at the roll-wave crests/agitated surfaces as well as droplet size distributions in the dispersed film boiling regime should depend on the gas and liquid physical properties and on the relative velocity. In view of the rather complicated nature of the droplet size dependence on these parameters, combined with knowledge that smaller droplets are short-lived due to vaporization, no definite conclusions concerning these effects can be made from the limited information available.

## V. CONCLUDING REMARKS

A visualization study of a simplified film boiling flow geometry, consisting of a Freon 113 liquid jet surrounded by a gas annulus, was carried out with the objective of determining the various flow regimes. It has been established that the axial flow pattern for this model of an inverted annular flow consists basically of four regions; namely, a nearly smooth section which begins at the nozzle exit, a rough wavy section with an intact liquid core, an agitated and a dispersed flow region, the latter being confined to the region near the exit of the test section. The axial limits of these flow regimes depend markedly on the relative velocity between the gas and the liquid. The axial extent of each flow zone ($L_B$), expressed in terms of the liquid jet nozzle diameter ($D_j$) as $L_B/D_j$, has been correlated using the liquid jet Reynolds and Weber numbers ($Re_j$ and $We_j$, respectively), and a modified gas Weber number based on relative velocity ($We_{g,rel}/\alpha^2$), where $\alpha$ is the void fraction.

Typical size distributions for droplets generated at the roll-wave crests (the maximum size being about 500 μm) as well as those formed in the dispersed flow regime (0.5-3 mm in diameter) have been presented.

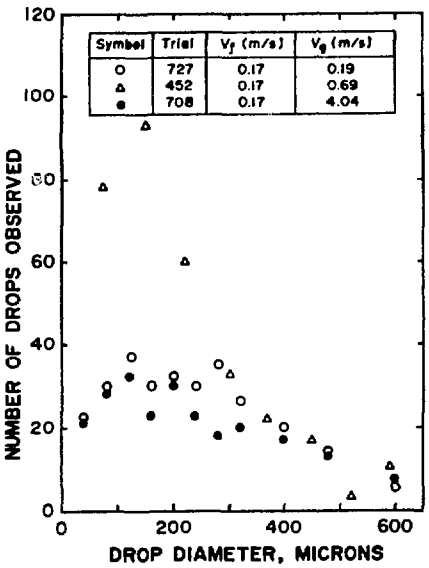


Fig. 7. Size Distribution for Droplets from Roll-wave/Agitated Surface

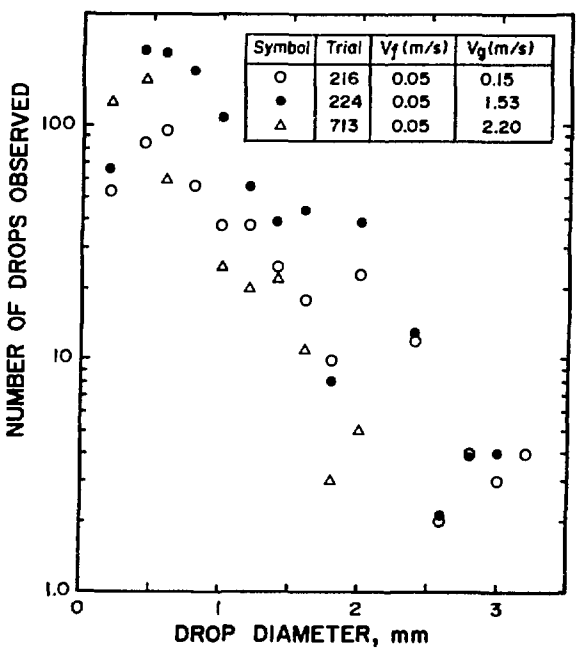


Fig. 8. Size Distribution for Droplets in the Dispersed Flow Regime

ACKNOWLEDGMENTS

This work was performed under the auspices of the U.S. Nuclear Regulatory Commission. The authors would like to express their sincere appreciation to Drs. Richard Lee and Novak Zuber for valuable discussions and support on the subject. N. T. Obot was supported as a Faculty Research Participant by the Argonne Division of Educational Programs.

REFERENCES

1. D. P. JORDAN, "Film and Transition Boiling," Advances in Heat Transfer, 5, 1968, 55-128.

2. L. D. CLEMMENTS and C. P. CIKVER, "Natural Convection Film Boiling Heat Transfer," Ind. Engng. Chem., 62, #9, 1970, 26-46.

3. E. K. KALININ, I. I. BERLIN, and V. V. KOSTYUK, "Film-Boiling Heat Transfer," Advances in Heat Transfer, 11, 1975, 51-197.

4. J. W. H. CHI and A. M. VETERE, "Two-Phase Flow During Transient Boiling of Hydrogen Determination of Nonequilibrium Vapour Fractions," Advan. Cryog. Engng., 9, 1964, 243-253.

5. J. W. H. CHI, "Cooldown Temperatures and Cooldown Time During Mist Flow," Advan. Cryog. Engng., 10, 1965, 330-340.

6. J. W. H. CHI, "Slug Flow and Film Boiling of Hydrogen," J. Spacecr. Rockets, 4, #10, 1967, 1329-1332.

7. E. K. KALININ, V. K. KOSHKIN, S. R. YARKHO, I. I. BERLIN, Y. S. KOCHELAEV, V. V. KOSTYUK, A. L. KUROLEV, and G. N. SDOBNOV, "Investigation of Film Boiling in Tubes with Subcooled Nitrogen Flow," Proc. 4th Intl. Heat Transfer Conf. Paper B.4.5, Paris (1970).

8. W. F. LAVERTY and W. M. ROHSENOW, "Film Boiling of Saturated Nitrogen Flowing in a Vertical Tube," ASME J. Heat Trans., 89, 1967, 90-98.

9. R. P. FORSLUND and W. M. ROHSENOW, "Dispersed Flow Film Boiling," ASME J. Heat Trans. 90, 1968, 399-407.

10. G. DEJARLAIS, "An Experimental Study of Inverted Annular Flow Hydrodynamics Utilizing an Adiabatic Simulation," NUREG/CR-3339, ANL-83-44, Argonne National Laboratory (1983).

11. G. DEJARLAIS, M. ISHII, and J. LINEHAN, "Hydrodynamic Stability of Inverted Annular Flow in an Adiabatic Simulation," Trans. ASME. J. Heat Trans., 108, 1986, 84-92.

12. M. ISHII and G. DEJARLAIS, "Flow Regime Transition and Interfacial Characteristics of Inverted Annular Flow," Nucl. Engng. Design, 95, 1986, 171-184.

13. G. DEJARLAIS and M. ISHII, "Inverted Annular Flow Experimental Study," NUREG/CR-4277, ANL-85-31, Argonne National Laboratory (1985).

14. M. ISHII and G. DEJARLAIS, "Flow Visualization Study of Inverted Annular Flow of Post Dryout Heat Transfer Region," Proc. 3rd Intl. Topical Mtg. on Reactor Thermal Hydraulics, Paper 1.C, Newport, RI (1985).

15. M. ISHII and G. DEJARLAIS, "Flow Visualization Study of Inverted Annular Flow of Post Dryout Heat Transfer Region, Nucl. Engng. Design, 99, 1987, 187-199.

16. R. W. GRAHAM, R. C. HENDRICKS, Y. Y. HSU, and R. FRIEDMAN, "Experimental Heat Transfer and Pressure Drop of Film Boiling Liquid Hydrogen Flowing Through a Heated Tube," Advan. Cryog. Engng., 6, 1961, 517-524.

17. YE. N. SINITSYN, G. W. MURATOV, and V. P. SKRIPOV, "The Surface Tension of F-11, 21 and 113," Heat Transfer-Soviet Research, 4, #4, 1972, 79.

18. M. ISHII and M. A. GROLMES, "Inception Criteria for Droplet Entrainment in Two-Phase Concurrent Film Flow," AIChE J., 21, #2, 1975, 308-317.

19. N. T. OBOT and M. ISHII, "Two-Phase Flow Regime Transition Criteria in Post-Dryout Region Based on Flow Visualization Experiments, NUREG/CR-4972, ANL-87-27, Argonne National Laboratory (1987).

## DISCLAIMER